7-1981

U-Pb Studies of Zircon Cores and Overgrowths, and Monazite: Implications for Age and Petrogenesis of the Northeastern Idaho Batholith

M. E. Bickford

R. B. Chase

B. K. Nelson

Robert Duncan Shuster
University of Nebraska at Omaha, rshuster@unomaha.edu

E. C. Arruda

Recommended Citation

U-Pb STUDIES OF ZIRCON CORES AND OVERGROWTHS, AND MONAZITE: IMPLICATIONS FOR AGE AND PETROGENESIS OF THE NORTHEASTERN IDAHO BATHOLITH[1]

M. E. BICKFORD, R. B. CHASE, B. K. NELSON,[2] R. D. SHUSTER, AND E. C. ARRUDA[3]

Department of Geology, University of Kansas, Lawrence, Kansas 66045
Department of Geology, Western Michigan University, Kalamazoo, Michigan 49008

ABSTRACT

U-Pb isotopic studies of zircons, many containing xenocrystic cores with euhedral overgrowths, and monazite from igneous rocks and metasedimentary inclusions of the northeastern Idaho batholith yield linear arrays on concordia diagrams. We interpret these as mixing lines between an old component (cores) and a young component (overgrowths and zircons without cores). The lower intercept of such arrays with concordia may yield the minimum age of the rocks if the overgrowths and zircons without cores are discordant, or the crystallization age if they are concordant. Monazites yield apparently concordant ages either equal or less than the lower intercept zircon ages. The samples studied yield lower intercept ages ranging from 73.5 ± 6 m.y. (foliated quartz diorite) to 46.5 ± 1 m.y. (feldspar megacryst granite); ages obtained are consistent with crosscutting relations observed in the field. Upper intercepts yield ages of 1700 to 2349 m.y. These are interpreted to indicate the mean age of xenocrystic zircon. Studies of zircons from xenolith suites indicate that they could represent the source of the old zircon component. The zircon and monazite results, the generally high initial $^{87}Sr/^{86}Sr$ ratios of the igneous rocks, and the isotopic composition of Pb in feldspar indicate that the magmas were derived anatectically from a continental crustal source or were extensively mixed with such old crust prior to or during emplacement.

INTRODUCTION

In an earlier paper (Chase et al. 1978) we reported preliminary results from a study of U-Pb systematics in zircons from rocks of the northeastern Idaho batholith and Rb-Sr systematics in these rocks and rocks of its metamorphic aureole. In that paper we presented evidence that the early phases of emplacement of igneous material may have begun about 82 m.y. ago and that the main plutons of the batholith were emplaced 66 ± 10 m.y. ago. These results were obtained by study of zircons which appeared to include two components, one 2075 ± 175 m.y. old and another whose age we believed to be the time of crystallization of the magmas. The presence of the old zircon

component, and the high values of the initial $^{87}Sr/^{86}Sr$ ratio in rocks we and others have studied from this region, suggested that older continental crust was significantly involved in the formation of these magmas. In this paper we will present the results of a much more detailed study whose goals were (1) to determine the age of emplacement of granitic rocks from the northeastern Idaho batholith and its border zone; (2) to identify the source of the "old" zircon component and to determine its age if possible; and (3) to consider the implications of these data for the source and subsequent evolution of batholith magmas.

Previous isotopic studies of rocks from the northern part of the Idaho batholith have included those of Reid et al. (1970, 1973), of Grauert and Hoffman (1973), and of Armstrong (1975a, 1975b, 1976, 1978) and Armstrong et al. (1977). Grauert and Hoffman were the first workers to recognize the presence of an old zircon component in their studies. Armstrong and his co-workers have provided and tabulated a wealth of K-Ar age data (most indicating ages of about 40–45 m.y.) and initial $^{87}Sr/$

[86]Sr values (most from within the Idaho batholith proper are greater than .708).

GEOLOGIC SETTING OF THE NORTHEASTERN IDAHO BATHOLITH

The Idaho batholith (fig. 1) is a composite group of plutons emplaced to the east of an inferred subduction zone (Hamilton 1969, fig. 4; 1976; Talbot and Hyndman 1975), north to northwest of the Sevier orogenic belt (Armstrong 1968, fig. 4), southwest of the Montana disturbed belt (Mudge 1970, fig. 1), and south of the Kootenay arc mobile belt in Canada (Harrison et al. 1974, p. 7). Igneous rocks in the northeastern sector of the batholith (fig. 2) have intruded quartzofeldspathic gneiss, pelitic schist, and calc-silicate gneiss which have been subjected to conditions of upper amphibolite-grade metamorphism and multiphase deformation, and remetamorphosed under lower-pressure conditions (Chase 1973, 1977; Nold 1974; Cheney 1975; Wehrenberg 1972).

The host rocks were penetratively deformed at least twice prior to batholitic intrusion. The earliest intrusive phase was quartz diorite on the periphery of the igneous complex, which was deformed and metamorphosed along with the host rocks prior to more voluminous intrusion of the main plutonic complex (Chase 1973). The main portion of the batholith contains many plutons whose contact locations are not known in detail. There are two principal granitic types, an earlier medium-grained granite and a later porphyritic gray granite distinguished by large potassium feldspar megacrysts. The emplacement sequence of these three plutonic types can be distinguished in the field by cross-cutting and xenolith distribution relationships.

The contact between batholith rocks and their metamorphic sheath is characterized by a wide zone of granitic sills and isolated blocks of country rock. Xenoliths are very abundant near the contact and decrease southwestward into the batholith over a zone that is about 2 km wide. Inclusions of quartzofeldspathic gneiss, pelitic schist, and calc-silicate gneiss are readily identified as fragments of the invaded country rocks. Other inclusions that are less abundant consist of biotite-rich schist and amphibolite. Amphibolite occurs in the country rocks as isolated boudins, but biotite schist is not common and may be present as exotic blocks from a greater depth than is represented by present exposures. Xenoliths of quartzofeldspathic gneiss and pelitic schist can be observed in various stages of digestion within igneous rocks, the extent of digestion commonly increasing into the batholith until only wisps of aligned mafic minerals and faint hints of lithologic layering indicate the position of an inclusion. Calc-silicate gneiss is evidently far less reactive, for such xenoliths typically show sharply angular borders and little evidence of incorporation into the magmatic rocks.

The northeastern Idaho batholith and its metamorphic envelope has been regionally uplifted to form a gneiss dome (Chase 1977; Chase and Talbot 1973). A zone of cataclasis has developed along the eastern margin of, and locally within, this dome which is up to 850 meters or more thick. Isolated parts of the dome have been affected by faulting, with mylonitization, retrograde metamorphism, and intrusion of felsic dikes in the fault zone. The large number of Eocene or younger K-Ar and Rb-Sr (biotite) and fission track (apatite) ages may be related to the thermal (Armstrong et al. 1977), hydrothermal (Criss and Taylor 1978), or uplift (Ferguson 1975) events associated with the doming, or some combination of these (Chase et al. 1978). Erosion to the present level has exposed the inner sector of the dome and the lower part of the batholith as well as the zone of cataclasis.

ISOTOPIC STUDIES OF ZIRCON AND MONAZITE

Rocks Sampled. — In accordance with the goals of this study, we sampled quartz diorite orthogneiss (sample A-33), medium-grained granite (sample IG-39), and granite with feldspar megacrysts (sample IG-38) in order
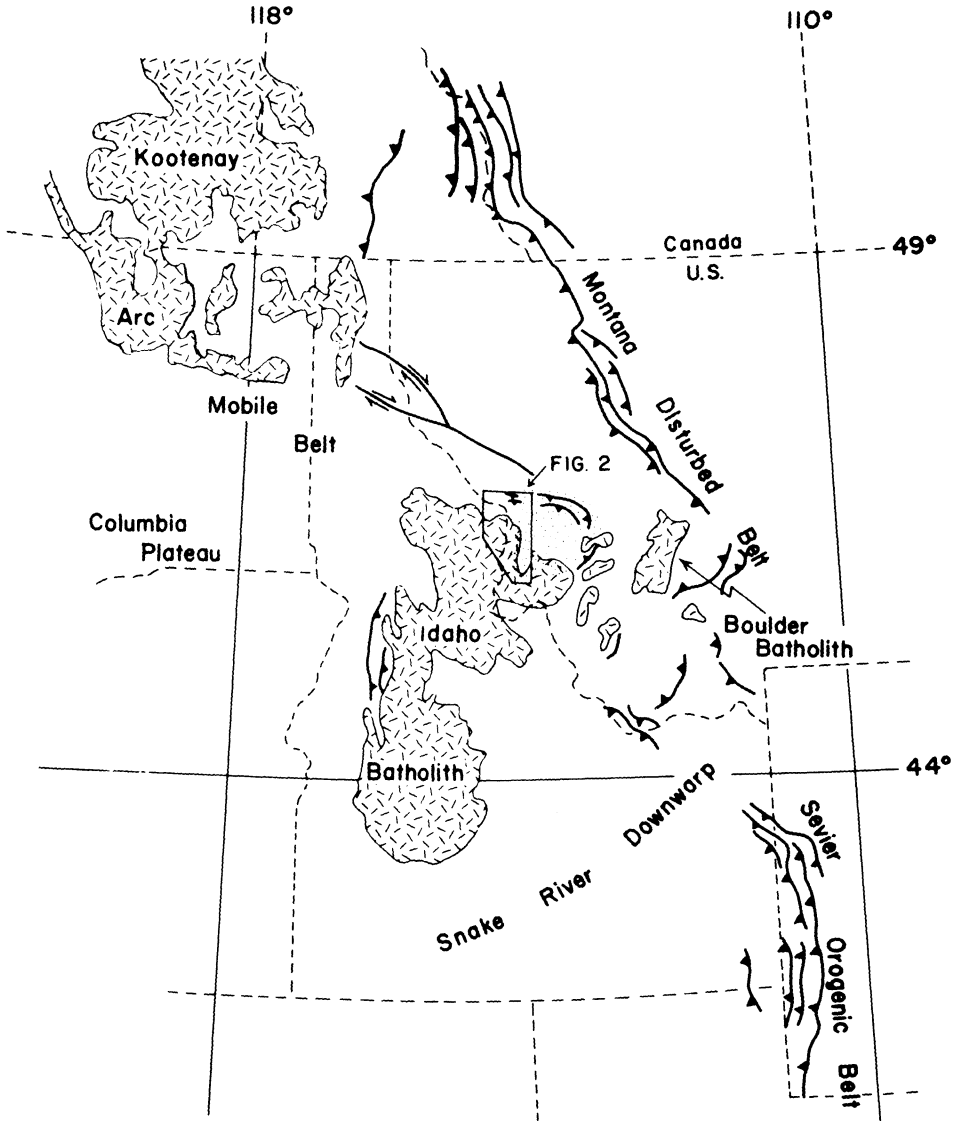
Fig. 1. – Tectonic setting of Idaho batholith. Sapphire block indicated by stippled pattern. Dash patterns indicate regions dominated by plutons. Zone of cataclasis is along western edge of Sapphire block.

to determine the age or ages of intrusive events. Additionally, we have studied samples of sheared granitic rocks (samples 79A15, 79A17, and 79A18) from within the zone of cataclasis in an attempt to place constraints upon the time of regional uplift.

We have studied a suite of inclusions (samples IGI-17, 19, 23, 28, and 35) collected from the contact zone inward into the batholith and ranging from only slightly to extensively reacted with the enclosing magmatic rocks, in order to see whether these rocks are the

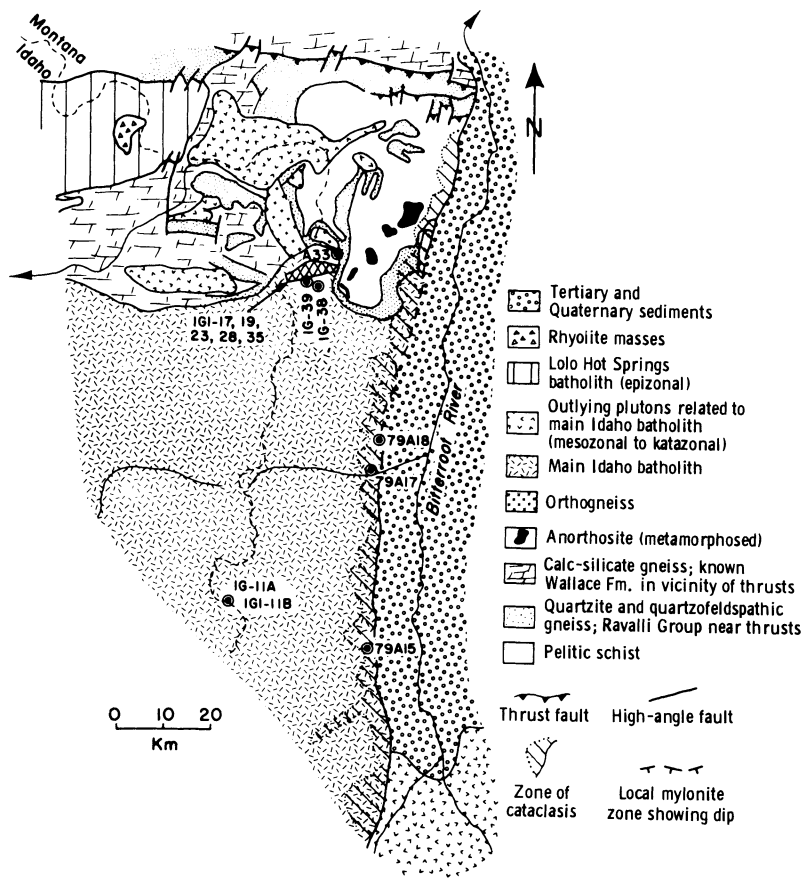Fig. 2. — Geologic map of northeastern border zone of Idaho batholith (enlargement of area outlined in fig. 1) showing location of samples studied. Map is adapted from Chase et al. (1978).

source of the old zircon component. Finally, we have studied a sample of granite (IG-11A), from a locality at least 20 km to the west of the contact, that enclosed a large inclusion of biotite schist (IGI-11B) to examine the contribution of such exotic inclusions to the old zircon component. The petrography of these samples is summarized in table 1, and the locality from which each was collected is shown on figure 2.

Nature of the Zircons and Monazite. — All of the samples we studied yielded abundant zircons and monazite. Under the binocular microscope the zircons are very clear. Those from the igneous rocks are mostly elongate and needle-shaped, with length-to-breadth

ratios of about 4 or 5. Zircons from the inclusions are also clear but are more variable in shape; those from the least digested inclusions (e.g. IGI-35) are somewhat rounded whereas those from the most completely digested inclusions (e.g., IGI-19) consist of numerous elongate, euhedral forms and a smaller proportion of rounded zircons. Monazite is a distinctive lemon-color, occurring mostly as anhedral grains. It is easily separated from zircon because of its higher magnetic susceptibility.

We also studied the zircon and monazite separates at high magnifications with a petrographic microscope. Viewed in oil immersion mounts under plane polarized

TABLE 1

Petrography and Modes of Igneous Rocks and Petrography of Quartzofeldspathic Gneiss Inclusions

	Igneous Rock Samples						
	Foliated Quartz Diorite	Granitic Rocks			Cataclastic Rocks		
Modes	A33	IG-11A	IG-38	IG-39	79A15	79A17	79A18
Quartz	37	24	35	21	18	26	36
Plagioclase	52	23	35	39	52	30	25
Plagioclase composition	An_{36}	An_{20-22}	An_{27-35}	An_{27-37}	An_{33}	An_{20}	An_{27}
K-feldspar	...	45	26	29	15	32	33
Biotite	11	6	4	10	10	12	Tr
Muscovite	Tr	Tr	Tr	Tr	...	Tr	6
Accessories	chlorite zircon apatite opaque sphene	chlorite zircon apatite opaque monazite	chlorite zircon apatite sphene opaque monazite	chlorite zircon apatite monazite opaque	sphene zircon apatite opaque garnet	zircon apatite opaque chlorite sphene rutile monazite	garnet zircon apatite
Textures	granoblastic to lepidoblastic; grain boundaries generally poly- gonal; virtually no secondary alteration.	hypidiomorphic-granular; somewhat seriate to porphyritic; grain boundaries generally poly- gonal with some suturing amongst quartz; minor show minor effects of cataclasis; minor secondary alteration.			cataclasite to mylonite augen gneiss; extensive sutured grain boundary relationships with local polygonal textures; much kinking and undulose extinction; slight sericite alteration.		

Quartzofeldspathic Gneiss Samples

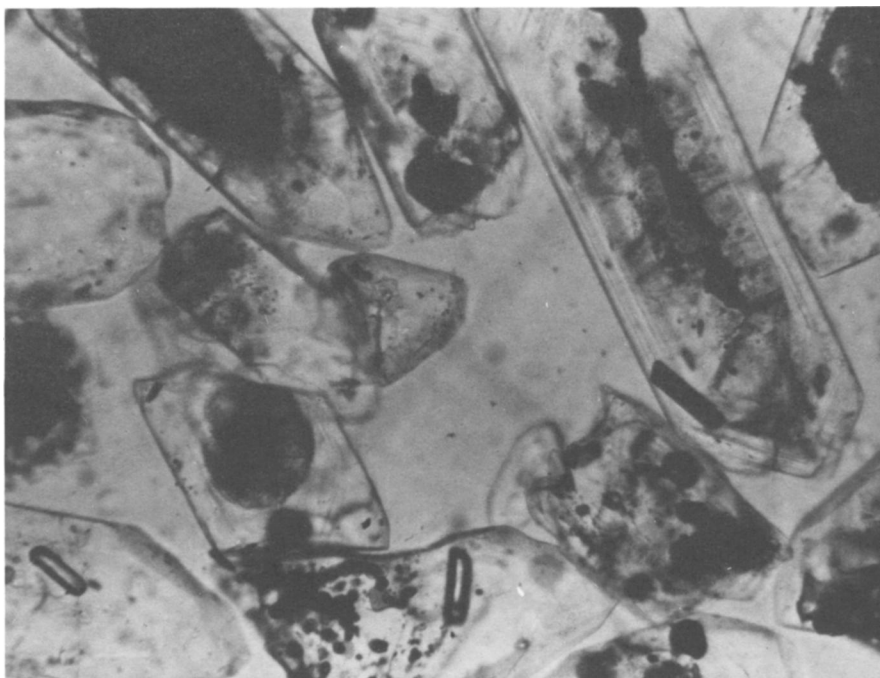|	
Composition	consists of quartz, feldspars, and biotite in varying proportions; may contain some of the following: muscovite, sillimanite, garnet, apatite, zircon, chlorite, sphene
Texture	sharply to diffusely layered; granoblastic to lepidoblastic; sutured grain boundaries; slight sericite alteration

Fig. 3. – Zircons from medium-grained granite (IG-39) showing altered cores and clear overgrowths. Plane light, 80X.

light, the zircon separates from all of our samples can be seen to contain many grains that have rounded to sub-rounded cores surrounded by euhedral overgrowths. Commonly the cores appear to be more altered or to have more tiny inclusions than the overgrowths (fig. 3), but this is not uniformly the case; some of the cores are quite clear. They are easily visible, however, because a strong Becke line forms at the boundary between the cores and the overgrowths.

Zircon separates from the least-digested inclusions consist almost entirely of rather rounded zircons with cores and overgrowths (fig. 4), but in the more completely digested inclusions the zircons include numerous elongate, euhedral zircons without cores as well as many that are more rounded and have cores (fig. 5). The igneous rocks contain far fewer zircons with cores and overgrowths than do the inclusions, but such zircons have been observed in every grain mount we have made from these rocks (fig. 6). In general, zircons from the igneous rocks, including those with cores, are more elongate and euhedral than those from the inclusions. Qualitatively, in both the inclusions and the igneous rocks, smaller zircons (i.e., those in the -200 mesh fraction) are more elongate and contain fewer grains with cores than the zircons in the coarser size fractions. All of these observations suggest that the cores were present in the metasedimentary inclusions, either as metamorphic zircons or as detrital zircons that were present in the sedimentary precursors of these rocks. The overgrowths presumably formed in response to a metamorphic episode whose relationship to the igneous activity is discussed below. The cores in the igneous rocks are presumably xenocrysts, acquired either from the source material of the melts or from contamination of the
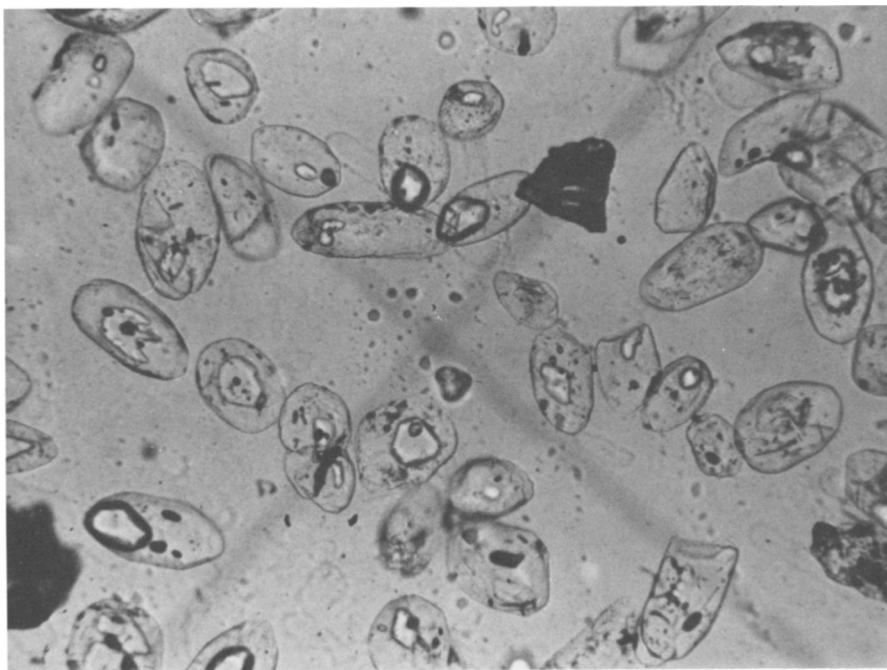
Fig. 4. — Rounded zircons with abundant cores from relatively undigested inclusion (IGI-28). Plane light, 80X.
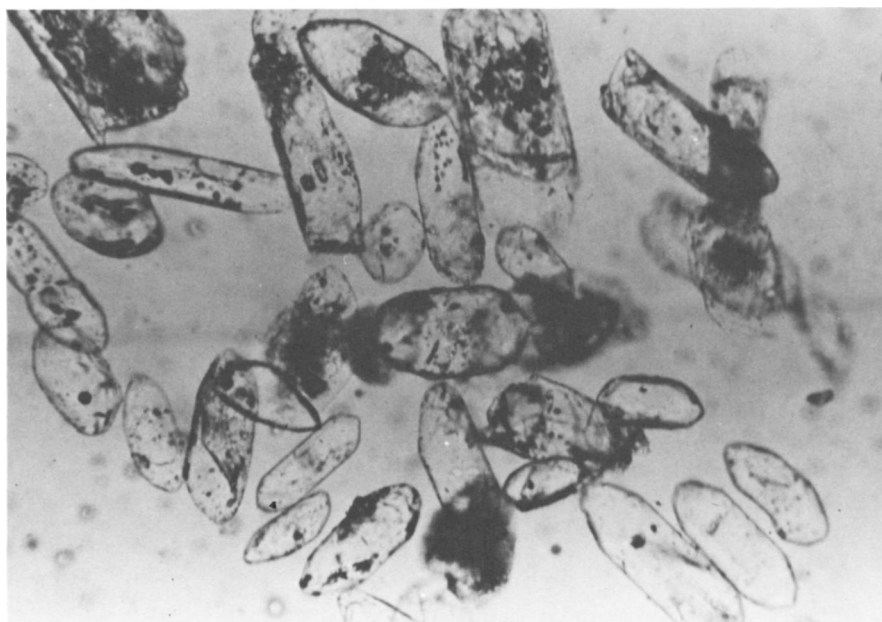

Fig. 5. — Zircons from more extensively digested inclusion (IGI-19) showing rounded forms commonly with cores and elongate forms commonly without cores. Plane light, 80X.
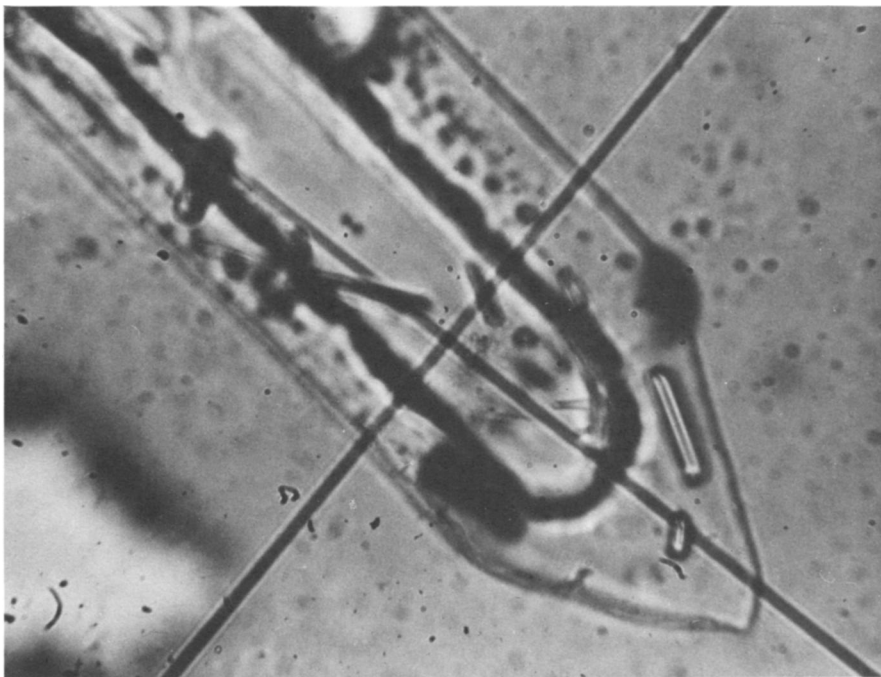
Fig. 6. — Zircons from feldspar-megacryst granite (IG-38) showing rounded core with euhedral overgrowth. Plane light, 400X.

magmas with country rocks. The overgrowths on these cores were evidently formed, along with most of the zircon that does not have cores, at the time of crystallization of the magmas. The question of the origin of the xenocrystic zircon cores in the igneous rocks has major implications for petrogenesis, and is discussed in detail following presentation of the isotopic data.

Analytical Results. — In this study we have determined concentrations and isotopic abundances of Pb and U from zircons and monazites by standard methods of mass spectrometry. The samples were dissolved in sealed teflon vessels and U and Pb separated according to the methods described by Krogh (1973). Mass spectrometry was done on an automated 9 inch radius instrument with on-line data reduction. Analyses of the NBS radiogenic Pb standard SRM 983 during the period of these analyses yielded the following values: $^{207}Pb/^{206}Pb =$

$.071209 \pm .000036$; $^{208}Pb/^{206}Pb = .013670 \pm .000032$; and $^{204}Pb/^{206}Pb = .0003672 \pm .0000065$; errors are given at 1σ. During the same period analytical blanks were < 5.0 ng for total Pb. The natural constants used were as follows: $\lambda^{238}U = 1.55125 \times 10^{-10}$/yr., $\lambda^{235}U = 9.8485 \times 10^{-10}$/yr., and atomic ratio $^{238}U/^{235}U = 137.88$. Analytical data are given in table 2.

Arrays of analytical data were interpreted by fitting lines to the data points using the least-squares-cubic method of York (1966) and then solving for the intercepts of the line thus determined with the concordia curve. The program used yields the slope and intercept of the best fit line and the uncertainties in these parameters at one standard deviation. Use of these uncertainties in the solution for the intercepts thus yields a maximum and minimum value, and these were taken as the error in the age determined at one standard deviation. As will be

seen, the lower intercept of the data arrays with concordia are as important in the interpretation of our results as the upper intercept, and this value was also determined.

It is also important to comment upon the methods we used to make common Pb corrections to the Pb-isotope data measured. As noted above, many of the zircons have rounded cores with sharply euhedral overgrowths. The data presented below shows that the zircon populations must consist of an old component, presumably the cores, and a young component, the overgrowths. Since we analyzed the zircons as mixtures of cores and overgrowths, it was not possible to determine whether the common Pb that was measured in the analyses came from the cores, the overgrowths, or both. We measured the isotopic composition of Pb in potassium feldspar from sample IG-38 (feldspar megacryst granite) carefully by doing a step-wise HF attack and measuring both the isotopic composition of Pb and the concentration of Pb and U for each step (Ludwig and Silver 1977 give an interesting account of the necessity for studying feldspars in this way). The data from this analysis are given in table 3 and show that the Pb is of essentially uniform composition throughout all of the dissolution steps, and that U concentrations are so small that no correction for in situ decay is required. We have used the composition of Pb determined in Step 6 of this analysis to make common Pb corrections on the assumption that it is representative of Pb that was in the magmas at the time of crystallization of overgrowths and zircons which have no cores. However, since we do not know how common Pb is distributed between cores and overgrowths, we also reduced the isotopic data on the assumption that all of the common Pb was in the cores. For this reduction, we used the isotopic composition of Pb according to the two stage growth model of Stacey and Kramers (1975), using 1750 m.y. as the mean age of the cores, except for sample 79A15 for which we used 2350 m.y. The results of reducing the data with these two different common Pb corrections are given in table 2.

In figures 7 through 10 and 13 through 15 the first age given is that resulting from reducing the data with the common Pb abundances measured from the feldspar; following in parenthesis is the age resulting from reduction with Stacey and Kramers model Pb. In the following text, however, we give only the age resulting from the feldspar Pb reduction, for in no case did the age resulting from the other reduction differ from this by an amount greater than the quoted uncertainties.

Foliated Quartz Diorite Orthogneiss. — The results of analysis of four zircon fractions and a monazite sample from quartz diorite orthogneiss are shown in fig. 7. Prior to analysis we separated the zircons into three fractions on the basis of size and we also obtained a fourth fraction, labeled "round," by hand picking those zircons which appeared to be the most stubby or rounded under a binocular microscope. The data points form a reasonably linear array, but not so linear as those from the other samples studied. The monazite sample yields a result that plots on concordia within analytical uncertainties, yielding a $^{206}Pb/^{238}U$ age of 54.5 ± 1 m.y. and a $^{207}Pb/^{235}U$ age of 58.7 ± 1 m.y. If one fits a line to the monazite point and all of the zircon data points, the result is a lower intercept of 53.6 ± 3 m.y. and an upper intercept of 1608 ± m.y. If a best-fit line is determined by the zircon data points alone, the result is a lower intercept of 73.5 ± 6 m.y. and an upper intercept of 1727 ± 40 m.y. Note that the smallest zircons (− 200 mesh) plot closest to the lower intercept whereas the "round" zircons, which are generally among the larger grains in the population, plot farthest from the lower intercept. In this array, there is little separation between the two intermediate size fractions (− 100 + 400 mesh and − 140 + 200 mesh).

Medium-Grained Granite and Feldspar-Megacryst Granite. — Figure 8 shows the results of analysis of monazite and zircon fractions from both the medium-grained granite (Sample IG-39) and the feldspar megacryst granite (Sample IG-38). As with

TABLE 2
U and Pb Analytical Data

Sample	U (ppm)	Pb (ppm)	Measured Ratios[a] $\frac{208Pb}{206Pb}$	$\frac{207Pb}{206Pb}$	$\frac{204Pb}{206Pb}$	Calculated Ratios[b] $\frac{207Pb}{206Pb}$	$\frac{206Pb}{238U}$	$\frac{207Pb}{235U}$	$\frac{207Pb}{235U}$ age [b]	$\frac{206Pb}{238U}$ age [b]
A-33										
"Round:	337.15	30.58	.33646	.17687	.005681	.09854 .09846	.06555 .06638	.89061 .90120		
−100 + 140	315.38	13.95	.30240	.13627	.003440	.08831 .08835	.03364 .03393	.40960 .41331		
−140 + 200	320.28	13.67	.21531	.11636	.002117	.08676 .08679	.03620 .03637	.43300 .43523		
−200	360.74	9.318	.25289	.12324	.003375	.07534 .07548	.02077 .02094	.21580 .21792		
Monazite	1765.3	69.04	4.02430	.08380	.002298	.05018 .05042	.00848 .00853	.05867 .05929	57.89 58.48	54.44 54.75
IG-39										
+ 100	776.54	124.02	.74809	.34390	.01777	.10021 .09975	.05965 .06348	.82420 .87304		
−100 + 140	891.67	65.65	.44223	.22663	.009559	.09452 .09447	.04220 .04339	.55000 .56520		
−140 + 200	933.57	49.72	.51258	.24426	.011278	.08681 .08701	.02794 .02890	.33441 .34670		
−200	1175.2	26.86	.44287	.19454	.008690	.07065 .07118	.01369 .01403	.13340 .13773		
Monazite	1909.3	146.46	10.24340	.08830	.002644	.04954 .04980	.00745 .00749	.05086 .05144	50.37 50.94	47.82 48.12
IG-38										
−100 + 200	1295.2	12.66	.16545	.09076	.001951	.06257 .06269	.00892 .00896	.07695 .07740		
−200 + 400	1086.7	8.80	.14918	.06901	.001140	.05230 .05238	.00773 .00775	.05576 .05595		
Monazite	1514.4	71.59	6.03026	.08031	.00207	.04995 .05014	.00741 .00741	.05105 .05146	50.60 50.96	47.6 47.8
79A-15										
+ 100	1134.0	27.55	.35113	.19214	.006530	.10283 .10394	.01626 .01669	.23056 .23924		
−100 + 140	1078.7	32.22	.69718	.30603	.015692	.08700 .09149	.01238 .01337	.14845 .16862		

TABLE 2 (Continued)

Sample	U (ppm)	Pb (ppm)	Measured Ratios[a]			Calculated Ratios[b]				
			$\frac{208Pb}{206Pb}$	$\frac{207Pb}{206Pb}$	$\frac{204Pb}{206Pb}$	$\frac{207Pb}{206Pb}$	$\frac{206Pb}{238U}$	$\frac{207Pb}{235U}$	$\frac{207Pb}{235U}$ age[b]	$\frac{206Pb}{238U}$ age[b]
79A-15 (Continued)										
−140 + 200	1280.3	23.96	.63647	.25164	.013299	.05929	.00878	.07181		
						.06453	.00934	.08310		
−200	1310.2	14.38	.37874	.13319	.005725	.04926	.00771	.05234		
						.05134	.00787	.05573		
79A-17										
Bulk	1187.0	15.74	.21396	.10532	.002459	.07009	.01157	.11184		
						.07019	.01163	.11252		
−100 + 140	936.42	41.89	.26623	.16276	.004758	.09709	.03486	.46628		
						.09697	.03521	.47081		
−140 + 200	1113.8	93.16	1.04087	.44691	.025794	.08687	.02062	.24693		
						.08748	.02306	.27809		
−200	1180.4	12.81	.22651	.09946	.002729	.05994	.00926	.07649		
						.06013	.00931	.07718		
79A-18										
+100	9001.4	138.72	.47366	.22851	.012239	.04922	.00828	.05621	55.52	53.17
						.05078	.00859	.06014	59.30	55.13
−100 + 140	10124.6	131.89	.34830	.17983	.008970	.04836	.00826	.05506	54.43	53.02
						.04949	.00848	.05782	57.08	54.40
−140 + 200	11076.3	133.32	.30579	.16375	.007891	.04805	.00812	.05383	53.23	52.16
						.04903	.00831	.05616	55.48	53.33
−200	9966.8	114.47	.27098	.15047	.006991	.04795	.00817	.05401	53.41	52.45
						.04881	.00833	.05605	55.37	53.47
IGI-17										
−100 + 200	954.1	18.16	.11270	.08441	.000759	.07360	.01842	.18687		
						.07362	.01844	.18718		
−200 + 400	1023.5	21.62	.22538	.12160	.003441	.07261	.01735	.17369		
						.07273	.01748	.17534		
IGI-19										
−100 + 400	1800.2	54.95	.11387	.08850	.000303	.08424	.02943	.34189		
						.08425	.02945	.34211		
IGI-19B										
−100 + 400	1920.8	58.90	.11713	.08929	.000372	.08406	.02951	.34198		
						.08407	.02952	.34222		

443

TABLE 2 (Continued)

Sample	U (ppm)	Pb (ppm)	Measured Ratios[a]			Calculated Ratios[b]				
			$\frac{^{208}Pb}{^{206}Pb}$	$\frac{^{207}Pb}{^{206}Pb}$	$\frac{^{204}Pb}{^{206}Pb}$	$\frac{^{207}Pb}{^{206}Pb}$	$\frac{^{206}Pb}{^{238}U}$	$\frac{^{207}Pb}{^{235}U}$	$\frac{^{207}Pb}{^{235}U}$ age[b]	$\frac{^{206}Pb}{^{238}U}$ age[b]
IGI-23										
−100 + 400	1668.0	30.18	.12181	.09300	.000968	.07932	.01719	.18794		
						.07934	.01722	.18834		
IGI-28										
−100 + 200	477.5	77.54	.19448	.11716	.001285	.09950	.14079	1.93150		
						.09947	.14120	1.93659		
−200 + 400	604.9	100.82	.17545	.10603	.000513	.09897	.15006	2.04771		
						.09896	.16031	2.18732		
IGI-28B										
−100 + 200	464.5	80.62	.21501	.12341	.001764	.09912	.14757	2.01685		
						.00908	.14812	2.02354		
IGI-35										
−100 + 400	496.7	107.71	.10431	.11120	.000127	.10948	.20703	3.12514		
						.10947	.20709	3.12583		
IGI-35B										
−100 + 400	498.7	106.71	.10468	.11052	.000091	.10928	.20494	3.08775		
						.10927	.20496	3.08800		
IGI11A										
+ 140	632.50	27.64	.58041	.27177	.013319	.08541	.02101	.24746		
						.08570	.02189	.25862		
−140 + 200	630.84	20.66	.48277	.23076	.010542	.08272	.01817	.20723		
						.08279	.01873	.21375		
−200	793.28	38.90	.92249	.39185	.022082	.08137	.01472	.16513		
						.08229	.01603	.18191		
Bulk	783.59	10.75	.15532	.09530	.001792	.06959	.01275	.12232		
						.06966	.01279	.12283		
Monazite	1145.4	92.14	9.24288	.07270	.001871	.04507	.00871	.05416		
						.04525	.00875	.05458		
IGI-11B										
−100	588.33	55.90	.28325	.16687	.004623	.10372	.07003	1.00145		
						.10359	.07087	1.01217		

TABLE 2 (Continued)

Sample	U (ppm)	Pb (ppm)	Measured Ratios[a]			Calculated Ratios[b]				
			$\frac{^{208}Pb}{^{206}Pb}$	$\frac{^{207}Pb}{^{206}Pb}$	$\frac{^{204}Pb}{^{206}Pb}$	$\frac{^{207}Pb}{^{206}Pb}$	$\frac{^{206}Pb}{^{238}U}$	$\frac{^{207}Pb}{^{235}U}$	$\frac{^{207}Pb}{^{235}U}$ age	$\frac{^{206}Pb}{^{238}U}$ age
IGI-11B (Continued)										
−100 + 140	598.89	58.19	.09719	.10944	.000215	.10649	.09375	1.37660		
						.10649	.09378	1.37697		
−140 + 200	599.70	47.96	.11087	.10813	.000337	.10350	.07632	1.08913		
						.10394	.07636	1.08965		
−200	656.12	22.89	.12661	.09940	.000444	.09320	.03326	.42744		
						.09320	.03328	.42766		
Bulk	629.89	48.00	.10449	.10688	.000225	.10379	.07327	1.04848		
						.10378	.07329	1.04876		
Monazite	1337.8	84.43	7.05587	.11169	.004503	.04536	.00821	.05136		
						.04588	.00830	.05252		

a Precision for measured ratios is ± .1% or better except for $^{204}Pb/^{206}Pb$ for which absolute precision is ± .00001. Concentrations of U and Pb ± 1%.
b Second set of calculated ratios, $^{207}Pb/^{235}U$ and $^{206}Pb/^{238}U$ ages calculated using 1750 m.y. common Pb or 2350 m.y. common Pb correction. See text for explanation. B fractions of IGI-19 (−100 + 200), and IGI-35 (−100 + 400) analyzed to demonstrate reproducibility.
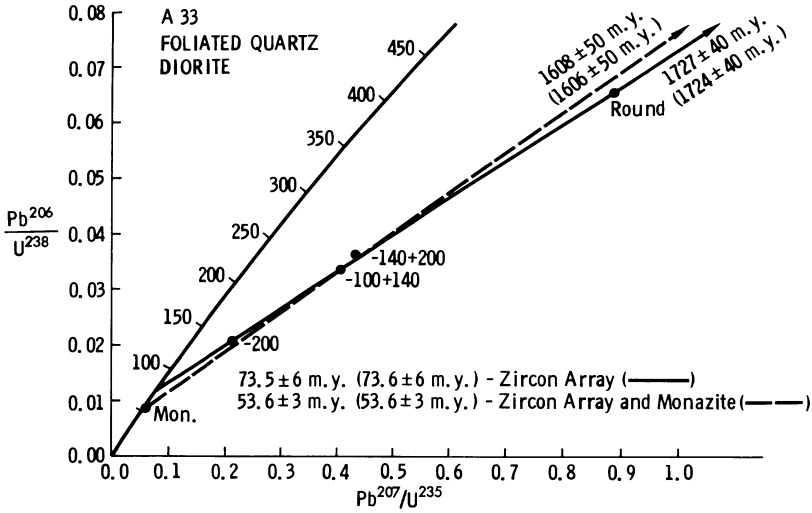
445

Fig. 7. — Concordia plot for zircons and monazite from foliated quartz diorite orthogneiss (A-33). Ages from regression of data reduced with common Pb abundances determined from K-feldspar; ages in parentheses determined from data reduced with model common Pb.
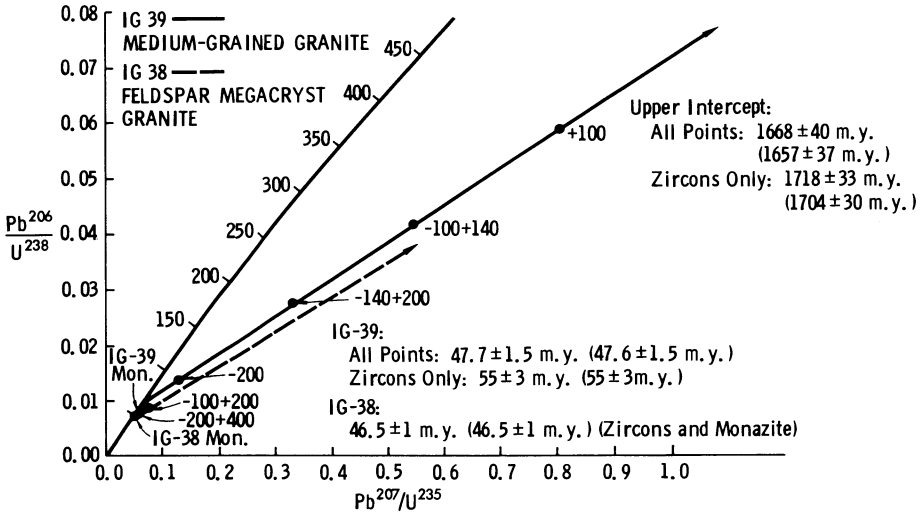

Fig. 8. — Concordia plot for zircons and monazite from medium-grained granite (IG-39) and feldspar-megacryst granite (IG-38). Ages from regression of data reduced with common Pb abundances determined from K-feldspar; ages in parentheses determined from data reduced with model common Pb.

the quartz diorite orthogneiss sample, we separated the zircons into size fractions prior to analysis, but we were unable to identify zircons in these rocks that were significantly "round" relative to the general zircon population.

Monazite from IG-39 is essentially concordant, yielding a $^{206}Pb/^{238}U$ age of 47.8 ± 1 m.y. and a $^{207}Pb/^{235}U$ age of 50.4 ± 1 m.y. A best-fit line through the zircon data points alone yields a lower intercept of 55 ± 3 m.y. and an upper inter-
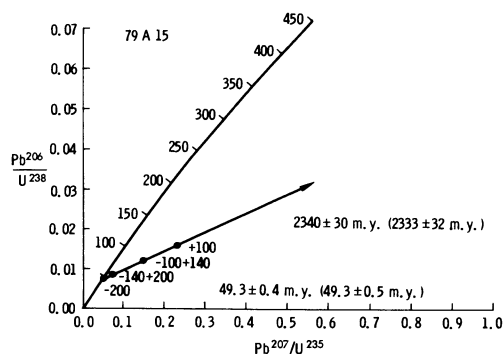
Fig. 9. — Concordia plot for zircons from sheared hornblende quartz monzonite (79A15). Ages from regression of data reduced with common Pb abundances determined from K-feldspar; ages in parentheses determined from data reduced with model common Pb.

cept of 1718 ± 33 m.y. If the monazite point is included in the array, the lower intercept is 47.7 ± 1.5 m.y. and the upper intercept is 1668 ± 40 m.y.

Monazite from IG-38 is also essentially concordant, yielding a $^{206}Pb/^{238}U$ age of 47.5 ± 1 m.y. and a $^{207}Pb/^{235}U$ age of 50.5 ± 1 m.y. The two zircon fractions from this sample do not yield the spread of values that the other samples do, but it is clear that they are displaced from the lower intercept along

a line that is below that determined by the IG-39 zircons. A line fit to the two zircon points and the monazite yields a lower intercept of 46.5 ± 1 m.y. and an upper intercept of 2013 ± 65 m.y.

Granite Rocks from the Zone of Cataclasis. — We studied suites of zircons from three samples from the zone of cataclasis on the eastern margin of the Idaho batholith. The results reviewed here are discussed in the companion paper by Chase et al. (in prep.). Sample 79A15 is from an intensely sheared, porphyritic, hornblende quartz monzonite. Analysis of data from a zircon suite from this sample yielded a lower intercept of $49.3 \pm .4$ m.y. and an upper intercept of 2340 ± 30 m.y. (fig. 9). Sample 79A17 is from a moderately sheared, medium-grained, biotite granodiorite. Its zircon suite yields a lower intercept of 47.7 ± 1.0 m.y. and an upper intercept of 1772 ± 11 m.y. (fig. 10). Sample 79A18 is from an intensely sheared leucogranite pegmatite. We separated four zircon size fractions from this rock, but all of them are essentially concordant, yielding $^{206}Pb/^{238}U$ ages ranging from 52 to 53 m.y. and $^{207}Pb/^{235}U$ ages ranging from 53 to 55 m.y.

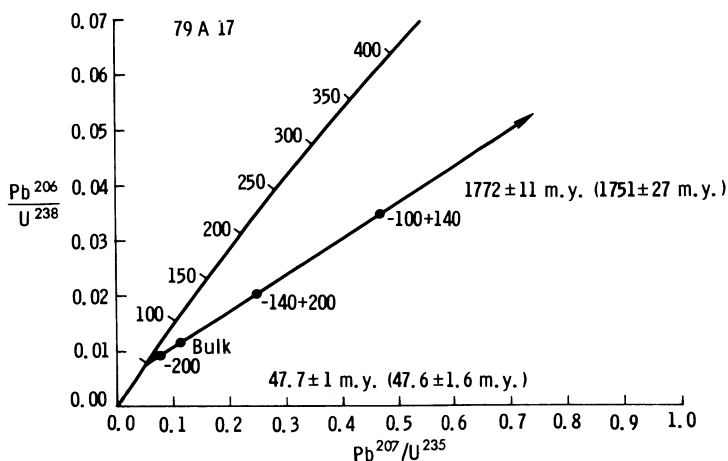*Inclusion Suite.* — The inclusions studied

Fig. 10. — Concordia plot for żircons from sheared biotite granodiorite (79A17). Ages from regression of data reduced with common Pb abundances determined from K-feldspar; ages in parentheses determined from data reduced with model common Pb.

Fig. 11. — Field photograph of extensively digested inclusion of quartzofeldspathic gneiss (IGI-17).

were all collected within the contact zone of the batholith with its carapace of high-grade metamorphic rocks. Our purpose in making this collection was to test whether the inclusions might represent the source of the "old" zircon component. We took inclusions of the invaded country rocks that were in various stages of reaction and digestion with the magmas of the batholith at the time that crystallization of the melts was complete. We anticipated that such a suite of inclusions might have varying proportions of an "old" zircon population and "new" overgrowths that would result in a range of values on a concordia plot. The inclusions collected are all quartzofelds-pathic gneiss; they range in degree of digestion from sample IGI-17 (fig. 11) which is extensively reacted and appears in the field as a "ghost" inclusion still showing banding and foliation of mafic constituents but with a quartzo-feldspathic matrix scarcely distinguishable from the enclosing granite, to samples IGI-28 and IGI-35 (fig. 12), quartzo-feldspathic gneiss fragments that are scarcely reacted with the enclosing granite and still preserve most of their structure and texture.

Samples IGI-19 and IGI-23 have field characteristics indicating intermediate degrees of reaction with magma.

For samples IGI-17, IGI-19, and IGI-28 we sized the zircon separates into $-100 + 200$ and $-200 + 400$ mesh fractions for analysis, but the zircons from the other inclusions were analyzed as the bulk population. The data are presented in fig. 13. It can be seen that the data points are not colinear. A chord fitted to the complete array yields a lower intercept of 62.3 ± 4.6 m.y. and an upper intercept of 1700 ± 37 m.y. If sample IGI-35 and IGI-35B are excluded from the least-squares analysis, the result is a lower intercept of 57.4 ± 3.5 m.y. and an upper intercept of 1629 ± 32 m.y. If samples IGI-28 (two size fractions) and IGI-28B are excluded, the lower intercept is 67 ± 5.5 m.y. and the upper intercept is 1771 ± 54 m.y. It is apparent that zircons from sample IGI-35, one of the least digested inclusions, plot reasonably close to the upper concordia intercept, suggesting that they have a large proportion of the "old" component, whereas zircons from IGI-17, one of the most extensively digested
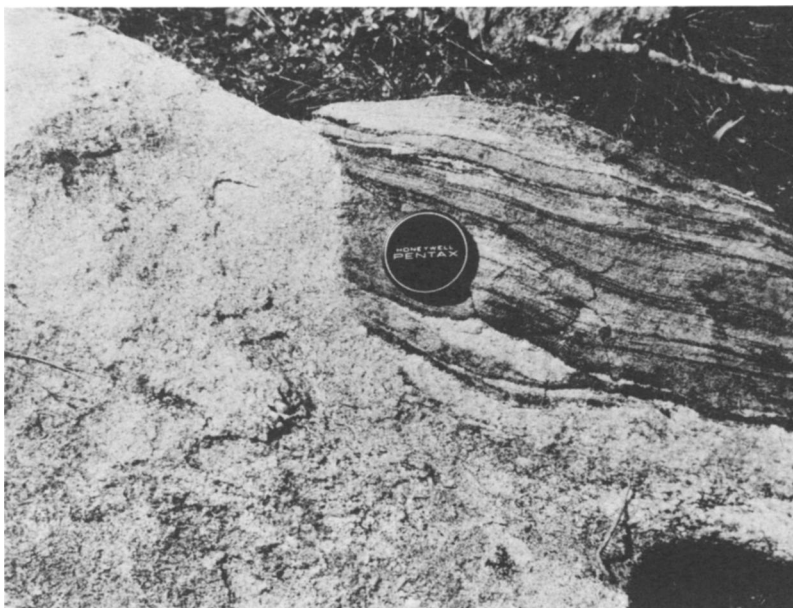
Fig. 12. — Field photograph of inclusion of quartzofeldspathic gneiss that has undergone little digestion (IGI-28).
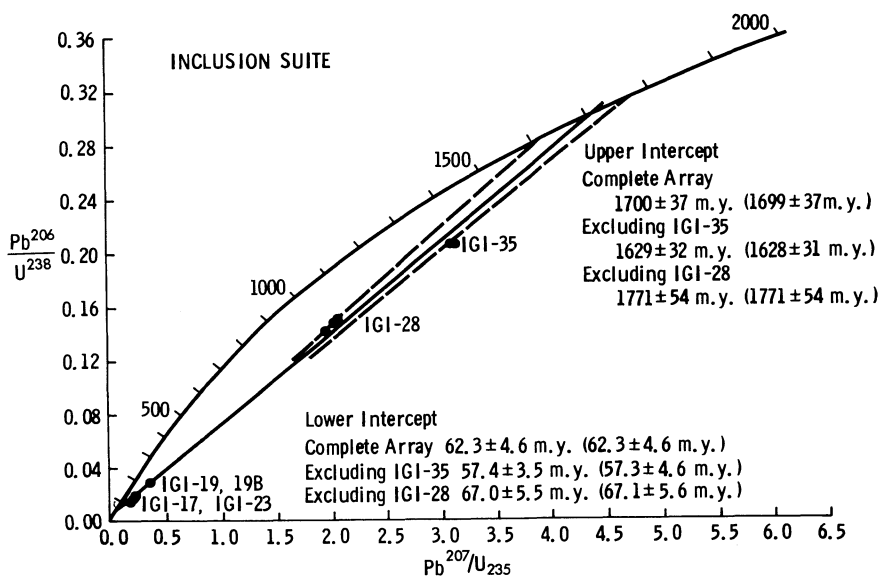

Fig. 13. — Concordia plot for zircons from inclusion suite. Ages from regression of data reduced with common Pb abundances determined from K-feldspar; ages in parentheses determined from data reduced with model common Pb.

Fig. 14. — Large inclusion of biotite schist and gneiss at Bear Pass locality (IG-11A and IGI-11B).
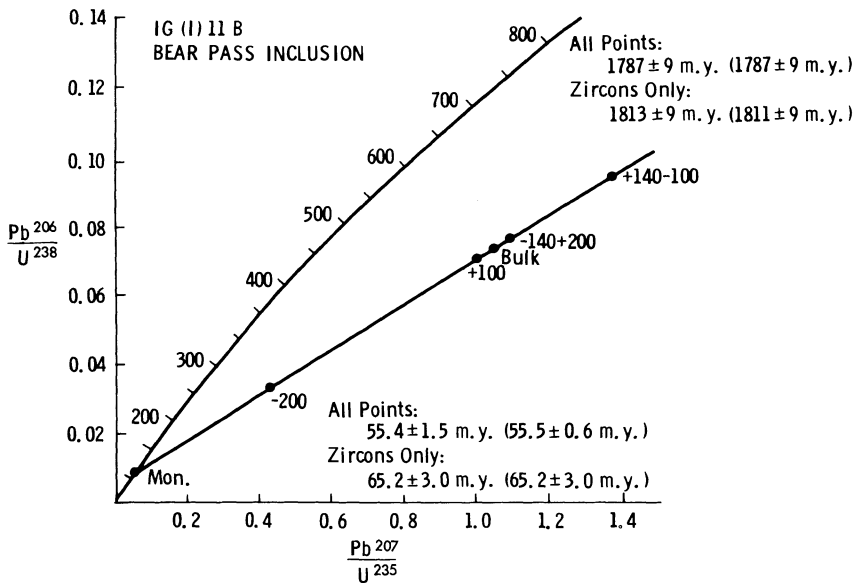

Fig. 15. — Concordia plot for zircons and monazite from inclusion at Bear Pass locality (IGI-11B). Ages determined from regression of data reduced with common Pb abundances determined from K-feldspar; ages in parentheses determined from data reduced with model common Pb.
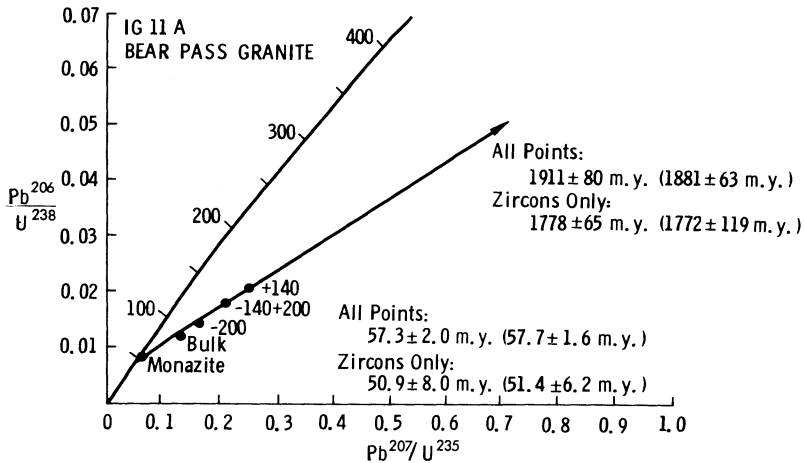
Fig. 16. — Concordia plot for zircons and monazite from granite at Bear Pass locality (IG-11A). Ages determined from regression of data reduced with common Pb abundances determined from K-feldspar; ages in parentheses determined from data reduced with model common Pb.

inclusions, plot very near the lower intercept, indicating a large proportion of the "new" component.

Granite-Inclusion Pair. — Sample IGI-11B was taken from an inclusion of biotite schist at Bear Pass (fig. 2). The inclusion, approximately $100 \, m^2$ in outcrop area (fig. 14) consists of both unreacted biotite schist and biotite schist that reacted with the enclosing granite magma. Taken alone, the zircon array from this inclusion yields a lower intercept of 65.2 ± 3 m.y. and an upper intercept of 1813 ± 9 m.y. If the data from the monazite analysis are included, the lower intercept in 55.4 ± 1.5 m.y. and the upper intercept is 1787 ± 9 m.y. (fig. 15). The monazite analysis clearly dominates the lower intercept age.

The granite which encloses this inclusion is represented by sample IG-11A. The zircon array, taken alone, yields a lower intercept of 50.9 ± 8.0 m.y., and an upper intercept of 1778 ± 65 m.y. If the monazite analysis is included the lower intercept is 57.3 ± 2.0 m.y. and the upper intercept is 1911 ± 80 m.y. (fig. 16).

DISCUSSION

Interpretation of Isotopic Data from Zircons and Monazite. — Our interpretation of the isotopic data from zircons and monazite is strongly influenced by our microscopic observation of rounded cores with clear, euhedral overgrowths in many of the zircons from both inclusions and igneous rocks. The isotopic data could be interpreted as indicating that the zircons from rocks of the Idaho batholith are of Precambrian age (about 1700 to 2300 m.y. old) but strongly discordant due to episodic or continuous Pb loss. This interpretation is clearly not consistent with the regional geologic relationships, which indicate emplacement of the Bitterroot lobe of the Idaho batholith in Late Cretaceous or Early Tertiary time. Thus we interpret the linear arrays of data points on concordia diagrams as mixing lines between two components in the zircon populations: an older component, presumably the rounded cores, and a younger component, presumably the euhedral overgrowths and the zircons without cores. Major questions in this interpretation are (1) whether the lower intercepts represent ages of crystallization, and (2) whether the upper intercepts represent the true age of the contaminating older zircons.

Lower Intercept Ages. — The meaning of the lower intercepts is particularly critical
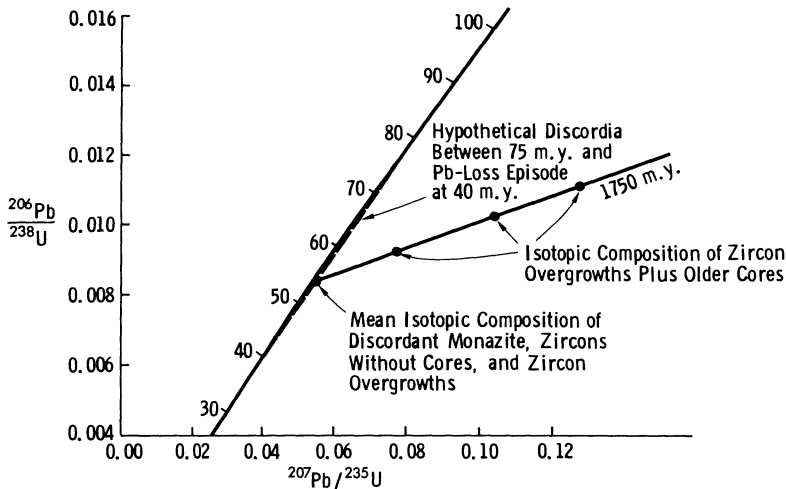
Fig. 17. — Hypothetical diagram to show effect of mixing discordant zircons, zircon overgrowths, and monazite with older cores.

for the geochronological aspect of our studies. The simplest interpretation is that the linear arrays are mixing lines between the age of the older component and the age of the younger component; in this case the lower intercept with concordia is the age of the young component. However, it is possible that the overgrowths and zircons without cores, although relatively young, are themselves discordant. Thus, as illustrated in figure 17, the lower end of the mixing line may be only the mean value of the Pb/U ratios for a population of discordant zircons which are actually older than the age indicated by the lower intercept.

We believe that our results for monazite are significant in the interpretation of the lower intercepts of the zircon arrays. Several recent authors have found that monazites yield concordant U-Pb ages (e.g., Aftalion and van Breemen 1980). Köppel and Grünenfelder (1975) argue that monazite ages generally indicate the peak of amphibolite facies metamorphism, whereas Purdy and Jäger (1976) believe that monazites have a maximum blocking temperature of 530°C.

In our study, the data from monazite plots on the concordia curve within analytical uncertainties. For sample IG-38, the youngest sample in terms of its field cross-cutting relationships and its zircon and monazite data, the monazite appears to plot at the zircon lower intercept (fig. 8). For sample IG-11A (fig. 16), the uncertainty in the zircon lower intercept age makes it indistinguishable from the monazite age. For all other samples for which we have monazite data (A-33, fig. 7; IG-39, fig. 8; IGI-11B, fig. 15) the monazite data indicate an age that is younger than the zircon lower intercept age, but none of the monazite ages is younger than the youngest zircon lower intercept age, i.e. the 46.5 ± 1 m.y. age of sample IG-38.

These results may be interpreted to mean that (1) the zircon arrays have preserved the crystallization ages of the rocks in the lower intercepts of the mixing lines, but that monazites are readily reset by younger thermal events, or (2) all of the rocks are older than any of the zircon lower intercept ages or the monazite ages, and that zircon overgrowths, zircons without cores, and monazites are all discordant (see fig. 17). In the latter case (interpretation 2) the monazite samples that yielded ages equal to the lower intercepts of the zircon arrays have behaved discordantly in bulk in the same manner as the young component

of the zircons, whereas those monazites that yielded younger ages than the lower intercepts of the zircon arrays are, in bulk, more discordant than the young component of the zircons.

Each of these interpretations of the data has some merit. The fact that the quartz diorite orthogneiss bodies are strongly foliated clearly indicates that they have a history not shared by the non-foliated granites. Thus, a crystallization age of about 73 m.y. (fig. 7) for our sample of quartz diorite orthgneiss is reasonable relative to ages of 46 to 56 m.y. for the non-foliated granites; monazite from this sample was presumably reset during intrusion of younger igneous rocks. The large inclusion at Bear Pass (IGI-11B; figs. 14 and 15) may have had a metamorphic history sufficiently intense to form overgrowths on old zircons, and perhaps nucleate new ones, 65 m.y. ago (before its incorporation in the granite). Its monazite, however, could have been reset about 55 m.y. ago during incorporation in granitic magma; the age of the monazite is the same as the enclosing granite (IG-11A, fig. 16) within analytical uncertainties. The monazite age of the medium-grained granite IG-39 (fig. 8) is consistent with its being reset by the intrusion of the feldspar megacryst granite IG-38 (fig. 8), a relation borne out by field observation.

The second interpretation, however, may also be related to some aspects of the geological history of the Idaho batholith. K-Ar and Rb-Sr ages of micas, and fission-track ages of apatite, record a thermal event that occurred 40–45 m.y. ago over a broad region of the batholith (Chase et al. 1978; Armstrong 1974, 1975, 1976; Ferguson 1975). The nature of this event is not known, but it has been suggested that it was associated with the last uplift of the batholith (Chase et al. 1978) or that it was associated with the Eocene-Oligocene Challis volcanic event (Armstrong 1974). In any case, it seems possible that this event caused Pb-loss in zircons and in monazite, as shown diagramatically in figure 17. If this is the case, the monazites are not really concord-

ant, but lie on discordia lines between the true age of the rocks (perhaps about 75 m.y.) and the 40 m.y. event; analytical uncertainties preclude distinguishing between truly concordant monazite ages and data points lying on such a discordia in the age range considered. The overgrowths on zircon cores, and zircons without cores, affected during this event would also lie on the discordia line, but the analytical points would be displaced on mixing lines towards the mean age of the cores. If this is the case, the lower intercept ages of zircon arrays and the monazite ages reported here may be interpreted only as the minimum ages of the rocks, and the true age of the Idaho batholith may never be known.

Our analytical data do not permit us to distinguish between the two interpretations discussed above. We argue here, however, that the first interpretation is more plausible and more in accord with the geological facts. First, the lower intercept ages of the rocks studied are completely consistent with their geologically observed relative ages. Thus, the quartz diorite orthogneiss is the oldest rock, having crystallized about 73 m.y. ago, the material in the Bear Pass xenolith underwent thermal metamorphism about 65 m.y. ago, the medium-grained granites were emplaced about 55 m.y. ago, and finally, the feldspar megacryst granite and the granites from the zone of cataclasis were emplaced between 49 and 46 m.y. ago.

If the ages indicated by the lower intercepts of the zircon arrays are not crystallization ages, it seems remarkable that the relative ages of the rocks, as indicated by field criteria, are preserved. The interpretation that all of the lower intercept U-Pb ages are minimum ages only, and are the result of mixing old cores with the mean value of discordant overgrowths and zircons without cores, requires that the monazite samples behave in such a manner that their mean discordance be either the same as the young zircon component, or that they be more discordant. Although we cannot prove that this was not the case, we believe that it is unlikely considering the differences in

chemical composition and crystal structure between zircon and monazite.

Upper Intercept Ages. – Upper intercept ages for zircon arrays alone range from a low of 1704 (IG-39; fig. 8) to 2340 m.y. (79A15; fig. 9). It seems clear that the xenocrystic zircons present as the observed cores were derived either from the source region of the magmas or from extensively admixed crustal material. These are important considerations, and will be treated below. In either case, however, the xenocrystic zircons may have come from older metasedimentary rocks or from older igneous rocks of greatly varying age. Thus, the upper intercept ages must be taken as the *apparent mean age* of the incorporated older zircons.

We studied the zircon populations of the inclusion suite from the contact zone to test the hypothesis that these inclusions represent the source of the contaminating zircons, either as representatives of contaminating material or as representatives of the source region of the magmas. The data presented in figure 13 indicates that the older component of the zircons in the inclusions does have about the same mean age, 1700 ± 37 m.y., as that in many of the granitic rocks. Thus, it seems likely that the inclusions do represent the source of the contaminating zircons. The fact that the zircons from the inclusion suite do not yield a colinear array, and that the upper intercept ages of the several zircon populations studied are variable, suggests that the old component is diverse in age, as might be expected in old metasedimentary rocks. The inclusion from Bear Pass (IGI-11B, figs. 14 and 15) was studied specifically to determine whether it might represent exotic material, perhaps derived from greater depths. Whatever its origin, its zircon array is strongly similar to that of the inclusion suite collected in the contact zone.

Other than the Bear Pass inclusion, the inclusions studied are identifiably derived from the high-grade metamorphic country rocks into which the igneous rocks of the Idaho batholith are intruded. These rocks are thought to be metamorphosed equivalents of the Proterozoic Belt Supergroup or possibly part of a pre-Belt terrane. The data given here only specify the mean age of the source regions of these metamsedimentary rocks, and thus do not indicate any specific source rock. It is of interest that the mean age of the old zircon component for so many of the granite samples and for the inclusion suite is about 1750 m.y. Rocks with radiometric ages ranging from 1,600 m.y. (Giletti 1966) to 2,750 m.y. (James and Hedge 1980) have been reported from the interiors of several nearby mountain ranges in Montana to the southeast of the region sampled for this study. Armstrong (1975) discussed the presence of 1500 m.y. old rocks in the Salmon River Arch which separates the Idaho batholith into its Bitterroot lobe and Atlanta lobe. It is possible that the approximately 1750 m.y. and 2350 m.y. upper intercept ages determined here result from mixtures of zircons from Archean rocks and those from younger Proterozoic rocks. The period 1700 to 1750 m.y. ago was, however, a time of extensive rock formation in other Proterozoic terranes, such as the northern Front Range in Colorado (Peterman and Hedge 1968; Stern and others 1977), central Wisconsin (Van Schmus 1978), and the Needle Mountains of southwestern Colorado (Bickford et al. 1969; Silver and Barker 1968). There may be rocks of this age within the crust in the vicinity of the Idaho batholith.

Petrogenetic Implications. – The presence of old, xenocrystic zircons in all of the igneous rocks we have studied strongly indicates that the magmas which formed them were derived by partial melting of an older continental crust or that magmas derived elsewhere were extensively contaminated with continental crustal material. The petrographic data available support this contention (Chase 1973). In the former case, the old zircon component is a refractory residue from melting, whereas in the latter it was derived during extensive incorporation of crustal material into magmas that may have been formed in the lower crust or in

the mantle. It is interesting that the experimental studies of Watson (1979) have shown that the solubility of Zr in granitic melts is strongly influenced by $(Na_2O + K_2O)/Al_2O_3$ such that in peraluminous melts Zr solubility is low, and less than 100 ppm Zr is necessary for zircon saturation. Thus the chemistry of the magmas may account for the presence of xenocrystic zircon in these rocks. In about eight years of working with zircons from subalkaline to peralkaline rocks in which Zr is theoretically more soluble in the magmatic phase, the senior author has never observed xenocrystic zircon.

The conclusion that the magmas that crystallized to form the igneous rocks of the northeastern border zone of the Idaho batholith were derived anatectically, or were extensively contaminated with older continental crust, is borne out by the published Sr isotope data (Chase et al. 1978; Armstrong et al. 1978) and our very preliminary Sr and common Pb isotope data. All of the igneous rocks we have studied have initial $^{87}Sr/^{86}Sr$ ratios greater than .7076, and most have ratios greater than .7100. The isotopic composition of common Pb in the potassium feldspar sample studied (table 3; from sample IG-38, which has the lowest initial $^{87}Sr/^{86}Sr$ of any sample we have yet studied), is not consistent with 55 m.y. old mantle Pb, as calculated on the model of Stacey and Kramers (1975). Rather, it is closer to the composition of approximately 300 m.y. Pb on the Stacey and Kramers model. These relationships strongly suggest that initial Sr and Pb isotopic compositions in the igneous rocks were the result of mixing of magmas whose Sr and Pb had more primitive isotopic compositions with older country rocks containing more radiogenic Sr and Pb. These suggestions will be tested in our future work through study of major and trace elements abundances in the igneous rocks, the country rocks, and the inclusions.

TABLE 3

Results of Stepwise HF Dissolution and Pb Isotopic Analysis of IG-38 K-feldspar

Step	Total Pb[a]	Total U[a]	$^{208}Pb/^{204}Pb$[b]	$^{207}Pb/^{204}Pb$[b]	$^{206}Pb/^{204}Pb$[b]
HNO₃ Leach	34.75	2.275	38.14	15.61	18.54
1	23.63	.085	38.22	15.58	18.19
2	30.10	.078	38.17	15.57	18.16
3	33.68	.153	38.21	15.57	18.18
4	31.86	.130	38.21	15.58	18.18
5	30.36	.003	38.11	15.55	18.15
6	25.61	.063	38.14	15.53	18.12

[a] Concentrations, ppm.
[b] Isotopic abundances ± .2% or better.

REFERENCES CITED

Aftalion, M., and van Breeman, O., 1980, U-Pb zircon, monazite, and Rb-Sr whole rock systematics of granitic gneiss and psammitic to semi-pelitic host gneiss from Glenfinnan, northwestern Scotland: Contrib. Mineral. Petrol., v. 72, p. 87–98.

Armstrong, R. L., 1968, The Sevier orogenic belt in Nevada and Utah: Geol. Soc. America Bull., v. 79, p. 429–458.

—— 1974, Geochronometry of the Eocene volcanic – plutonic episode in Idaho: Northwest Geology, v. 3, p. 1–15.

—— 1975a, Precambrian (1500 m.y. old) rocks of central Idaho; the Salmon River Arch and its role in Cordilleran sedimentation and tectonics: Am. Jour. Sci., v. 275-Z (Tectonics and mountain ranges), p. 437–467.

—— 1975b, The Geochronometry of Idaho (part I): Isochron/West 14, p. 1–50.

—— 1976, The geochronometry of Idaho (part II): Isochron/West 15, p. 1–33.

——; Taubeneck, W. H.; and Hales, P. O., 1977, Rb-Sr and K-Ar geochronometry of Mesozoic granitic rocks and their Sr isotopic composition, Oregon, Washington, and Idaho: Geol. Soc. America Bull., v. 88, p. 387–411.

Bickford, M. E., Wetherill, G. W., and Barker, Fred, and Lee-Hu, Chin-Nan, 1969, Precambrian Rb-Sr chronology in the Needle Mountains, southwestern Colorado: Jour. Geophys. Res., v. 74, p. 1660–1676.

Chase, R. B., 1973, Petrology of the northeastern border zone of the Idaho batholith; Bitterroot Range, Montana: Montana Bur. Mines and Geol. Memoir 43, 28 p.

—— 1977, Structural evolution of the Bitterroot dome and zone of cataclasis: in Geol. Soc. America Field Guide No. 1, Rocky Mountain Sec. Meeting, University of Montana, Missoula, Montana, p. 1–24.

——; Bickford, M. E., and Tripp, S. E., 1978, Rb-Sr and U-Pb isotopic studies of the northeastern Idaho batholith and border zone: Geol. Soc. America Bull., v. 89, p. 1325–1334.

——, and Talbot, J. L., 1973, Structural evolution of the northeastern border zone of the Idaho batholith, western Montana: Geol. Soc. America Abs. with Prog., v. 5, p. 471–472.

Cheney, J. T., 1975, Kyanite, sillimanite, phlogopite, cordierite layers in the Bass Creek anorthosites, Bitterroot Range, Montana: Northwest Geology, v. 4, p. 77–82.

Criss, R. E., and Taylor, H. P., Jr., 1978, Regional $^{18}O/^{16}O$ and D/H variations in granitic rocks of the southern half of the Idaho batholith and the dimensions of the giant hydrothermal systems associated with the emplacement of the Eocene Sawtooth and Rocky Bar plutons:

Geol. Soc. America Abs. with Prog. v. 10, p. 384.

Ferguson, J. A., 1975, Tectonic implications of some geochronometric data from the northeastern border zone of the Idaho batholith: Northwest Geology, v. 4, p. 53–58.

Giletti, B. J., 1966, Isotopic ages from southwestern Montana: Jour. Geophys. Res., v. 71, p. 4029–4036.

Grauert, B., and Hofmann, A., 1973, Old radiogenic lead components in zircons from the Idaho batholith and its metasedimentary aureole: Carnegie Inst. Wash., Year Book 72, p. 297–299.

Hamilton, W., 1969, Mesozoic California and the underflow of Pacific mantle: Geol. Soc. Americ Bull., v. 80, p. 2409–2430.

—— 1976, Tectonic history of west-central Idaho: Geol. Soc. America Abs. with Prog., v. 8, p. 378–379.

Harrison, J. E., Griggs, A. B., and Wells, J. D., 1974, Tectonic features of the Precambrian Belt basin and their influence on post-Belt structures: U.S. Geol. Survey Prof. Paper 886, 15 p.

James, H. W., and Hedge, C. E., 1980, Age of the basement rocks of southwest Montana: Geol. Soc. America Bull., v. 91, p. 11–15.

Köppel, V., and Grünenfelder, M., 1975, Concordant U-Pb ages of monazite and xenotime from the central Alps and the timing of the high temperature Alpine metamorphism, a preliminary report: Schweiz. Mineral Petrogr. Mitt., v. 55, p. 129–132.

Ludwig, K. R., and Silver, L. T., 1977, Lead-isotope inhomogeneity in Precambrian igneous K-feldspars: Geochim. Cosmochim. Acta, v. 41, p. 1457–1471.

Mudge, M. R., 1970, Origin of the disturbed belt in northwestern Montana: Geol. Soc. America Bull., v. 81, p. 377–392.

Nold, J. L., 1974, Geology of the northeastern border zone of the Idaho batholith, Montana and Idaho: Northwest Geology, v. 3, p. 47–52.

Purdy, J. W., and Jäger, E., 1976, K-Ar ages of rock-forming minerals from the central Alps: Mem. Inst. Geol. Min. Univ. Padova, v. 30, 31 p.

Reid, R. R., Greenwood, W. R., and Morrison, D. A., 1970, Precambrian metamorphism of the Belt Supergroup in Idaho: Geol. Soc. America Bull., v. 81, p. 915–918.

——; Morrison, D. A., and Greenwood, W. R., 1973, The Clearwater orogenic zone: a relict of Proterozoic orogeny in central and northern Idaho: Belt Symposium, Dept. of Geology, University of Idaho, Moscow, Idaho, p. 10–56.

Silver, L. T., and Barker, F., 1967, Geochronology of Precambrian rocks of the Needle Mountains,

southwestern Colorado: part I, U-Pb zircon results (Abs.): Geol. Soc. America Abs. for 1967, Spec. Pap. 115, p. 204–205.

Stacey, J. S., and Kramers, J. D., 1975, Approximation of terrestrial lead isotope evolution by a two-stage model: Earth Planet. Sci. Letters, v. 26, p. 207–221.

Stern, T. W., Phair, G., and Newell, M., 1977, Boulder Creek batholith, Colorado: part II, isotopic age of emplacement and morphology· of zircon: Geol. Soc. America Bull., v. 82, p. 1615–1634.

Talbot, J. L., and Hyndman, D. W., 1975, Consequence of subduction along the Mesozoic continental margin west of the Idaho batholith: Geol. Soc. America Abs. with Prog., v. 7, p. 1290.

Van Schmus, W. R., 1978, Geochronology of the southern Wisconsin rhyolites and granites: Geoscience Wisconsin, v. 2, p. 19–24.

Watson, E. B., 1979, Zircon saturation in felsic liquids: experimental results and applications to trace element geochemistry: Contrib. Mineral. Petrol., v. 70, p. 407–419.

Wehrenberg, J. P., 1972, Geology of the Lolo Peak area, northern Bitterroot Range, Montana: Northwest Geology, v. 1, p. 25–32.

York, D., 1966, Least-squares fitting of a straight line: Can. Jour. Physics, v. 44, p. 1079–1086.